Dalton Transactions

Accepted Manuscript

ROYAL SOCIETY OF CHEMISTRY

www.rsc.org/dalton

Journal Name Dalton Transactions Dynamic Article Links ►

Cite this: DOI: 10.1039/c0xx00000x

www.rsc.org/xxxxxx

ARTICLE TYPE

Gas sensing and electrochemical properties of tetra and octa 2*H*-chromen-2-one substituted iron(II) phthalocyanines

Selçuk Altun[a], Efe Baturhan Orman[a], Zafer Odabaş[a], Ahmet Altındal[b]* and Ali Rıza Özkaya[a]**

Received (in XXX, XXX) Xth XXXXXXXXX 20XX, Accepted Xth XXXXXXXXX 20XX
DOI: 10.1039/b000000x

The synthesis of novel alpha tetra, beta tetra and beta octa 4-(4-methoxyphenyl)-8-methyl-coumarin-7-oxy, and beta octa 4-chloro-5-(4-(4-methoxyphenyl)-8-methylcoumarin-7-oxy substituted iron(II) phthalocyanines has been achieved by the reaction of corresponding phthalonitriles with iron(II)acetate. The compounds were characterized by elemental analysis, FT-IR, UV–*vis*, and MALDI-TOF mass spectrometry. The reduction and oxidation properties of the compounds were identified by voltammetric and *in situ* spectroelectrochemical measurements. The gas sensing behavior of the spin coated films of the differently substituted iron(II) complexes towards CO_2, CO and SO_2 were investigated at various temperatures between 300 K and 500 K. While exposure to SO_2 had no considerable influence on the sensor current, the presence of CO and CO_2 gases led to large increase in sensor currents. The effect of relative humidity on the CO and CO_2 sensing capability of the spin coated films was also studied. The results showed that the presence of water vapor, acting as interference gas, causes a decrease of the CO_2 sensitivity, but an increase of the CO sensitivity of the sensors. The experimental adsorption data were analyzed using Elovich kinetic model. Linear regression analysis results show that Elovich equation provides the best correlation for the CO_2 and CO adsorption processes under humid conditions. However, the experimental data deviated considerably from the theoretical model in dry atmosphere.

1. Introduction

Phthalocyanines (Pcs) are macrocyclic compounds with the highly conjugated planar hetero aromatic 18π–electron system. These compounds display highly thermal and chemical stability and unique physical, electrochemical and photochemical properties.[1,2] Pcs usually have a blue or green colour due to the intense $\pi-\pi^*$ electronic transitions associated with the π-conjugated ring system. The previous studies on the physical, chemical, electronic and electrochemical properties of Pc compounds clearly showed that these properties, determining their applicability in technology can be improved by the molecular modification through careful selection of the central metal ion and utilization of substituents with varying numbers (tetra and octa substitution) and different connecting positions (peripheral and non-peripheral substitution).[3,4] Iron(II) Pc is a special complex for Pc researchers because it is the first metallo Pc complex discovered by accident in 1928[5,6] and its derivatives display excellent catalytic activities for various chemical, biochemical and electrochemical reactions.[7-12] In addition, iron(II) Pcs have been receiving increasing interest because of its close analogy to the iron porhyrin and blood hemine.[13] Considerably high chemical inertness and thermal stability of the FePc and other transition MPc complexes led the researchers to explore the technological utility of the metallo Pcs as display devices, data storage, chemical sensors, gas sensors, biosensors,[14] solar cells, organic light emitting devices, photovoltaic cells, semiconductive materials and photodynamic therapy.[6,15-21]

On the other hand, coumarin (2H-1-benzopyran-2-one) derivatives are a group of natural compounds found in a variety of plant sources.[22] Many natural and synthetic coumarin derivatives are widely used as laser dyes,[23] chemosensors for metal detections, pH sensors, liquid crystals and organic non-linear optical materials, due to their high emission yield, excellent photostability and extended spectral range.[24] Therefore, the combination of coumarin and Pc functional groups into a single hybrid compound via a suitable synthetic methodology is expected to produce highly functional compounds with intriguing physicochemical properties. Accordingly, numerous studies have been carried out with the goal of moderating their properties and optimizing their performance for advanced materials.[23,25-27] Furthermore, a set of study reported by our group included the synthesis, characterization and investigation of electrical, electrochemical, *in situ* spectroelectrochemical, photochemical and photophysical properties of alpha tetra, beta tetra and beta octa 4-(4-methoxyphenyl)-8-methyl-coumarin-7-oxy, and beta octa 4-chloro-5-(4-(4-methoxyphenyl)-8-methylcoumarin-7-oxy substituted metal-free, zinc(II), cobalt(II) and Mn(III) Pcs.[4,28-30] These studies showed that the metal in the central position in these compounds remarkably change their properties.

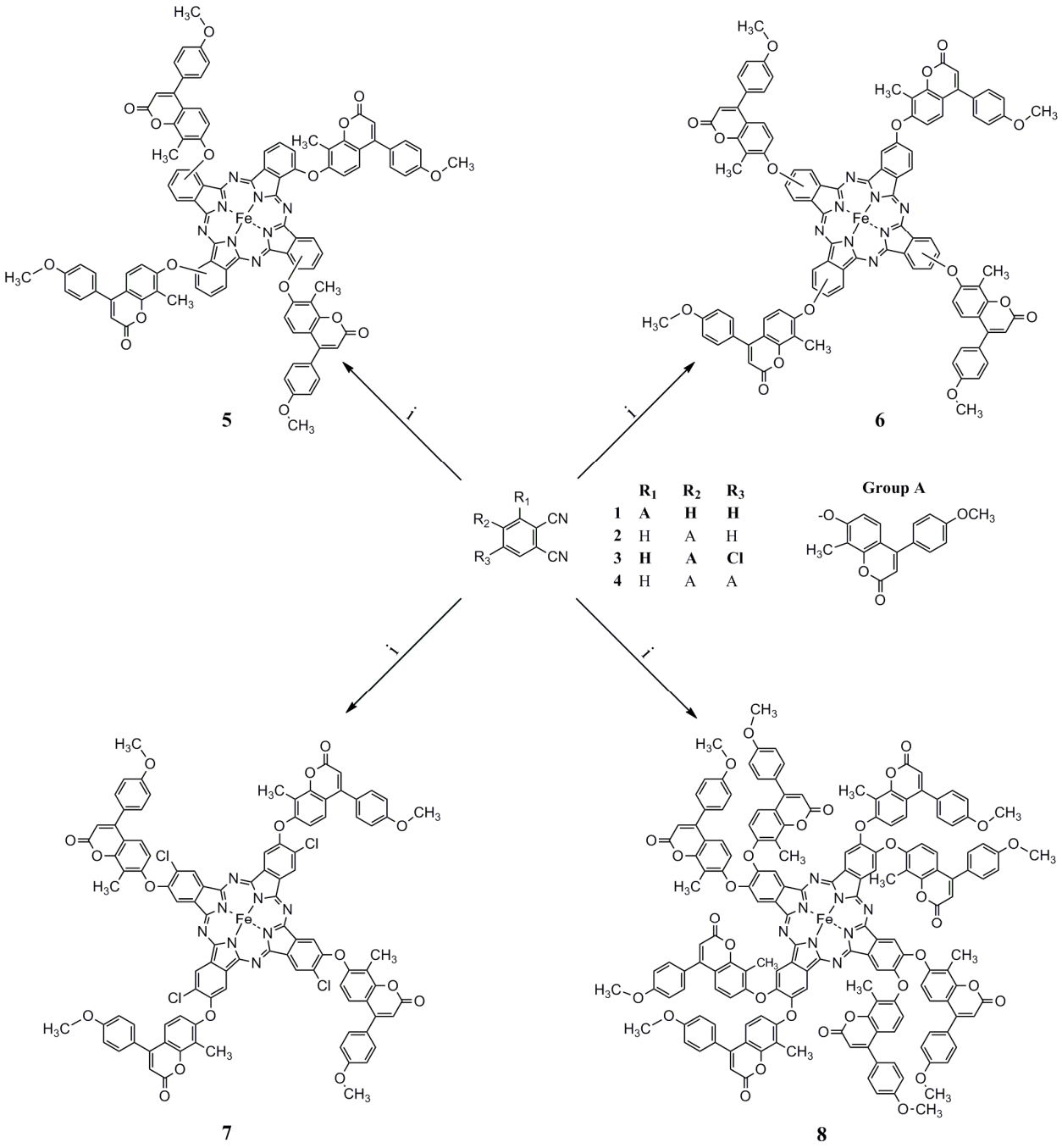

Scheme 1 Synthesis of **5**, **6**, **7** and **8**. Reagents and conditions: i. b) $Fe(CH_3COO)_2$, dimethylformamide, N_2, 420 °C, 20 min.

In this study, the preparation of alpha tetra, beta tetra and beta octa 4-(4-methoxyphenyl)-8-methyl-coumarin-7-oxy, and beta octa 4-chloro-5-(4-(4-methoxyphenyl)-8-methylcoumarin-7-oxy substituted iron(II) Pcs has been presented for the first time (Scheme 1). The characterization of the compounds was achieved by elemental analysis, UV–vis, FT-IR and matrix assisted laser desorption/ionization-time of flight (MALDI-TOF) mass spectrometry. These complexes display both metal- and Pc ring-based redox processes.[31,32] In most cases, it is not possible to identify the nature of the redox processes, i.e., whether it occurs at the ring or on the metal center, using only electrochemical techniques such as voltammetry and controlled-potential coulometry. However, the use of *in situ* UV–vis spectro-electrochemistry, a technique applied by the combination of UV–vis spectroscopy with the electrochemical technique of controlled-potential electrolysis, and then the evaluation of the results together with those of voltammetric methods make the identification of the nature of the redox processes possible.[31]

Thus, in this study, the effect of the position and the number of substituents on the redox and aggregation properties of the complexes has been examined by cyclic voltammetry and *in situ* UV–vis spectroelectrochemistry.

The studies in the literature show that carbon dioxide is responsible for about two thirds of the greenhouse effect, and thus plays a primary role in global warming.[33] It may also cause respiratory organ disease. Due to high importance of the detection and the control of its concentration, much effort has been made on the development of the sensing methods for CO_2 gas. For these reasons, sensing properties of the thin films of the synthesized complexes for CO_2, CO and SO_2 were also investigated in this study. The kinetics of the adsorption of CO_2 and CO gases onto the compounds were analyzed using Elovich equation.

2. Experimental Section

2.1. Material and methods

FT-IR and electronic spectra were recorded on a Shimadzu FTIR-8300 (KBr pellet) and a Shimadzu UV–1601 spectrophotometer, respectively. Elemental analyses were performed by the Instrumental Analysis Laboratory of TUBITAK–Ankara. Mass spectra were acquired on an Autoflex III MALDI-TOF mass spectrometer (Bruker Daltonics, Germany) equipped with a nitrogen UV–Laser operating at 337 nm in reflectron mode with average of 50 shots.

2.2. Sample and matrix preparation

The compound, α-cyano-4-hydroxycinnamic acid (ACCA) was prepared in THF at a concentration of 10 mg/mL as matrix. MALDI samples were prepared by mixing sample solutions (2 mg/mL in chloroform) and matrix solution (1:10 v/v) in a 0.5 mL eppendorf® micro tube. Finally, 0.5 µL of this mixture was deposited on the sample plate, dried at room temperature, and then analyzed.

2.3. Synthesis

2.3.1. General procedure for synthesis of iron(II)Pcs (5, 6, 7 and 8)

A mixture of one of the phthalonitrile compounds (**1**, **2**, **3** or **4**) (4.50 x10^{-4} mol) and $Fe(CH_3COO)_2$ (0.087 g, 5 x10^{-4} mol) was powdered in a quartz crucible and transferred in a reaction tube. 0.30 mL of DMF was added to this reaction mixture, and then the mixture was heated in the glass tube for 20 minutes under dry N_2 atmosphere at 420 ^oC. After cooling to room temperature, 3 mL of DMF was added to the residue to solve the product. The reaction mixture was precipitated by adding acetic acid. The precipitate was filtered and washed with acetic acid, water, ethanol and acetonitrile for 12 hours respectively in the soxhlet apparatus. The crude product was purified by column chromatography with silica gel eluting with a gradient of chloroform-THF mixture up to 5% THF.

2.3.1.1. *1(4),8(11),15(18),22(25)- tetra(4-(4-methoxyphenyl)-8-methylcoumarin-7-oxy)phthalocyaninatoiron(II)* ***5***

The compound is soluble in dichloromethane (DCM), chloroform ($CHCl_3$), THF, DMF, and dimethylsulfoxide (DMSO). Mp >300^o C. Yield: 15.20 mg (7.62%). Anal calculated for $C_{100}H_{64}FeN_8O_{16}$: C 71.09%; H 3.82%; N 6.63%; found C, 69.91%; H, 3.75%; N, 6.81%. IR (KBr pellet) ν_{max}/cm^{-1}: 742, 833, 956, 1025, 1044, 1083, 1115, 1175, 1244, 1325, 1366, 1421, 1480, 1511, 1582, 1603, 1723, 2837, 2927, 3000, 3069. MALDI-TOF-MS: m/z 1689.67 $(M)^+$, 1706.75 $(M+H_20)^+$. UV–vis (DMSO): λ_{max} (nm), (log ε): 315 (5.53), 605 (4.88), 669 (5.23).

2.3.1.2. *2(3),9(10),16(17),23(24)-tetra(4-(4-methoxyphenyl)-8-methylcoumarin-7-oxy)phthalocyaninatoiron(II)* ***6***

The compound is soluble in DCM, chloroform, THF, DMF, DMSO. Mp >300^o C. Yield: 18.3 mg (9.16%). Anal calculated for $C_{100}H_{64}FeN_8O_{16}$: C 71.09%; H 3.82%; N 6.63%; found C, 70.89%; H, 4.01%; N, 6.74%. IR (KBr pellet) ν_{max}/cm^{-1}: 747, 832, 955, 1080, 1174, 1248, 1366, 1469, 1511, 1595, 1728, 2837, 2929, 3065. MALDI-TOF-MS: m/z 1689.63 $(M)^+$, 1706.72 $(M+H_20)^+$. UV–vis (DMSO): λ_{max} (nm), (log ε): 328 (5.32), 631 (5.12).

2.3.1.3. *2,9,16,23-tetra(chloro)-3,10,17,24-tetra(4-(4-methoxy-phenyl)-8-methylcoumarin-7-yloxy)phthalocyaninatoiron(II)* ***7***

The compound is soluble in DCM, chloroform, THF, DMF, DMSO. Mp >300^o C. Yield: 39.1 mg (19.66%). Anal calculated for $C_{100}H_{60}Cl_4FeN_8O_{16}$: C 65.73%; H 3.31%; N 6.13%; found C, 65.57%; H, 3.43%; N, 5.95%. IR (KBr pellet) ν_{max}/cm^{-1}: 744, 838, 897, 1045, 1085, 1178, 1250, 1369, 1410, 1456, 1513, 1604, 1731, 2854, 2926, 3007, 3071. MALDI-TOF-MS: m/z 1827.26 $(M)^+$, 1850.25 $(M+Na)^+$. UV–vis (DMSO): λ_{max} (nm), (log ε): 316 (5.56), 594 (4.74), 631 (5.04), 656 (5.13).

2.3.1.4. *2,3,9,10,16,17,23,24-octa(4-(4-methoxy-phenyl)-8-methylcoumarin-7-yloxy) phthalocyaninatoiron(II)* ***8***

The compound is soluble in DCM, chloroform, THF, DMF, DMSO. Mp >300^o C. Yield: 19 mg (9.60%). Anal calculated for $C_{168}H_{112}FeN_8O_{32}$: C 71.79%; H, 4.02%; N, %3.99; found C, 71.61%; H, 3.88%; N, 4.11%. IR (KBr pellet) ν_{max}/cm^{-1}:747, 836, 888, 1087, 1178, 1252, 1369, 1398, 1438, 1513, 1599, 1732, 2905, 2956, 2999, 3071. MALDI-TOF-MS: m/z 2810.74 $(M)^+$, 2833.81 $(M+Na)^+$. UV–vis (DMSO): λ_{max} (nm), (log ε): 344 (5.24), 595 (4.60), 657 (5.09).

2.4. Electrochemical and in situ spectroelectrochemical measurements

Voltammetric measurements were carried out with a PAR VersoStat II model potentiostat/galvanostat controlled by an external PC and utilizing a three-electrode configuration at 25 ˚C. The working electrode was a Pt plate with a surface area of 0.10 cm^2. A Pt spiral wire served as the counter electrode. A saturated calomel electrode (SCE), separated from the bulk of the solution by a double bridge was employed as the reference electrode. Electrochemical grade tetrabutylammonium perchlorate (TBAP) in extra pure DMSO was employed as the supporting electrolyte at a concentration of 0.10 mol dm^{-3}. High purity of N_2 was used for deoxygenating the solution at least 15 minutes prior to each run and to maintain a nitrogen blanket during the measurements. *In situ* spectroelectrochemical measurements were carried out by an Ocean Optics HR2000+ diode array spectrophotometer equipped with the potentiostat/galvanostat and utilizing an optically transparent thin layer (OTTLE) cell as three-electrode configuration at 25° C. The working electrode was transparent Pt gauze. A Pt wire counter electrode and a SCE reference electrode separated from the bulk of the solution by a double bridge were used.

2.5 Gas sensing experiment

The devices suitable for gas sensing measurements have been prepared by spin-coating the solutions of Fe(II)Pc compounds as chemiresistive thin films with a thickness between 60 and 600 nm over the electrode arrays. The electrodes used in the gas sensing measurements consisted of an interdigital array of Au metal electrodes which were photolitographically patterned and etched to provide 10 fingers pairs of electrodes with a width of 50 μm and a space of 50 μm between the adjacent electrodes. A series of films with different thickness have been deposited by varying the number of coatings and the concentration of coating solutions. An elipsometric technique was used to measure the thicknesses of the films. The substrate temperature during the deposition process was held constant at room temperature (~25 °C) to maintain constant film morphology across all sensors. The gas sensing properties of the coating material were tested in a cylindrical chamber of Teflon, 8 cm long and 4 cm diameter, through which a gas could be passed. The concentration of a target gas was well adjusted by mixing it with the reference gas. All sensing experiments were carried out by using two different carrier gases, dry nitrogen and air, with the aim of clarifying the effect of carrier gas on the gas sensing performance. The carrier gases had a purity level of 99% and water content less than 3%. The concentration of the target gas was varied from 200 to 1000 ppm by using mass flow controllers (MKS Inst. Co.). In order to overcome the complicating effect of an interface gases, such as O_2 and water vapour, and achieve the activation of a sensor before the measurement, the carrier gas was introduced first in the test chamber to clean the interface gas molecules adsorbed on the surface of sensing layers. Then, a small amount of analyte molecules was introduced into the test chamber to activate the sensing layer. Finally, pure carrier gas was introduced again to clean the analyte molecules left in the chamber and on the surface of the sensing layers. After these treatments, the sensing properties of the synthesized Pc films were investigated as a function of temperature and analyte concentration. The sensor current was measured by applying a constant bias of 1 V to each device and monitoring the current with a Keithley Model 6517 A electrometer. Sensor responses were reported as the change in sensor current at constant voltage on dosing with analytes. A typical gas sensing experiment consisted of repeated exposure to target gases and subsequent purging with carrier gas to reset the baseline. To avoid any fluidic and background pressure effect, the total flow rate was adjusted as 100 standard cubic centimeter (sccm) during both in exposure and purging experiments. Gas sensing data were recorded using an IEEE-488 data acquisition system incorporated to a personal computer. The results obtained under these conditions were reproducible with an uncertainty smaller than 4%.

3. Results and Discussion

3.1. Synthesis and characterization

The starting materials, phthalonitrile derivatives (1-4), have been synthesized by the method reported previously in the literature.[4,28,29] The syntheses of iron(II) Pcs bearing (4-methoxyphenyl)-8-methylcoumarin-7-oxy and/or chloro substituents have been achieved with the yields of 7.62% for **5**, 9.16% for **6**, 19.66% for **7**, and 9.60% for **8**. The characterization of the new products was carried out by the co-evaluation of the data obtained from the FT-IR, UV–vis, and MALDI-TOF mass spectrometry and elemental analysis. The results are consistent with the proposed structures (Table S1).

The FT-IR spectra of **5-8** showed Ar-O-Ar, -C=C-, -C=O, $-CH_3$ and aromatic –CH- peaks within the ranges of 1244-1251, 1595-1604, 1723-1732, 2837-2956 and 3066-3071 cm^{-1}, respectively. In addition, the absence of -C≡N peaks within the range of 2229-2235 cm^{-1} in the spectra clearly indicated that starting compounds **1-4** could be converted to **5-8** (Table S1).

The UV–vis spectra of **5-8** in DMSO showed characteristic Q band and vibrational absorptions within the range of 656-669 and 594-605 nm, respectively, which can be attributed to the π→π* transitions from the highest occupied molecular orbital (HOMO) to the lowest unoccupied molecular orbital (LUMO) of the Pc ring. The Q-band absorptions within the range of 656-669 nm below 700 nm confirm that the central metal in the complexes are in the form of Fe(II). The B bands within the UV range of 294-311 nm were due to the transitions from the deeper π levels to the LUMO (Fig. S1 and Table S1). The comparison of the UV–vis spectra of **5-8** in DMSO with each other suggests that the spectra of **7** and **8** exhibit approximately a blue shift of 15 nm in the Q-band in comparison with those of **5** and **6**. It appears that the π-π* transition energy from the HOMO to the LUMO of the Pc ring increases with increasing number of electron withdrawing chlorine or coumarin substituents since the complexes **7** and **8** have more electron withdrawing group than the others. The spectra of **6-7** showed characteristic H-aggregated bands approximately at 630 nm. The aggregation tendency of these compounds can be attributed to their planar molecular shape.

The molecular ion peaks for **5-8** appeared at 1689.67, 1689.63, 1827.26 and 2810.74 Da, respectively. Beside the molecular ion peaks of the complexes, water adducts for **5** and **6**, sodium ion adducts for **6**, **7** and **8**, and potassium adduct for **6** were also monitored. The intensities of the sodium adduct peaks of **5** and **8** were equal to those of their molecular ion peaks, which indicates that sodium selectivity of these complexes is higher than that of the others. All high resolved experimental peaks matched perfectly the theoretical peaks of the complexes determined by isotropic software calculation. Thus, MALDI-TOF mass spectroscopy analyses confirmed the structures of all Pc samples (Fig. S2).

3.2. Electrochemistry

Electrochemical and *in situ* spectroelectrochemical measurements of the complexes **5-8** were performed in de-aerated DMSO/TBAP electrolyte system on a Pt working electrode. Table 1 lists the assignment of the redox couples and determined electrochemical data, which included half-wave peak potential ($E_{1/2}$), anodic to cathodic peak potential separation (ΔE_p), and difference between the first oxidation and reduction potentials ($\Delta E_{1/2}$). ΔE_p values at 0.010 V s^{-1} scan rate were within the range of 0.050 to 0.200 V reflecting reversible or quasi-reversible behaviour. Controlled-potential coulometry measurements suggested that all redox processes involve the transfer of one electron per molecule.

Figure 1 shows the cyclic voltammograms of alpha tetra coumarin substituted Fe(II)Pc (**5**) in DMSO-TBAP at various scan rates. The complex **5** undergoes a one-electron oxidation and two one-electron reductions. The first reduction R1 and oxidation

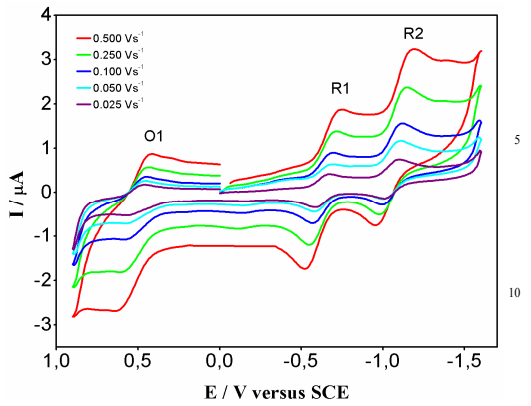

Fig. 1 Cyclic voltammograms of **5** (5.00 x 10^{-4} mole dm^{-3}) at various scan rates on Pt in DMSO/TBAP.

O1 processes are probably metal-based whereas R2 process is ring-based.

In situ UV–*vis* spectroelectrochemical measurements were also carried out to assign the redox processes, especially the first reduction and the first oxidation processes of **5** certainly. Fig. 2 represents the spectral changes during the first reduction of **5** at -0.85 V *vs.* SCE, corresponding to the redox process labelled R1 in Fig. 1. The Q band at 671 nm decreases in intensity and two new bands at 518 and 810 nm appear. The formation of the new band at 518 nm and the shifting of the Q band indicate the formation of $[Fe(I)Pc(-2)]^-$ species, confirming the CV assignment of the couple R1 to $Fe(II)Pc(-2)/[Fe(I)Pc(-2)]^-$ process.[34] During the further reduction at −1.40 V *vs.* SCE, the Q band at 671 nm decreases, while a new band is recorded 646 nm (Fig. 2B). These spectral changes at the potential of the couple R2 are characteristics for a ring-based reduction in Fe(I)Pc complex and confirm our voltammetric assignment of this process to $[Fe(I)Pc(-2)]^-/[Fe(I)Pc(-3)]^{2-}$.[34] During the potential application of +0.75 V, shifting of the Q band from 671 to 700 nm and the formation of a band at 512 nm indicate a metal-based process which is assigned to $[Fe(II)Pc(-2)]/[Fe(III)Pc(-2)]^+$ (Fig. 2C).

Cyclic and square wave voltammograms of beta tetra coumarin substituted complex **6** in DMSO are shown in Fig. 3. The compound gives three reductions and two oxidations signals with anodic to cathodic peak separations within the range of 0.050-0.200 V at 0.010 Vs^{-1} scan rate (Table 1). The cathodic component of the first reduction couple is split into two peaks (R1 and R1′). Considerably small difference between the O1' and O1" couples also suggest that these couples correspond to splittting of the metal-based first oxidation process, i.e., the O1" couple is not due to the oxidation of singly oxidized species of **6**. Furthermore, the voltammetric peaks are considerably rounded. All these observations indicate clearly the presence of aggregated species in the solution. The aggregation tendency of this beta-substituted complex can be attributed to its planar nature. The splitting and/or broadness of the redox processes of various metal phthalocyanine complexes due to their aggregation have been observed previously in the literature.[34-36]

In situ UV–vis spectroelectrochemical measurements may provide support for the existence of the aggregated species and

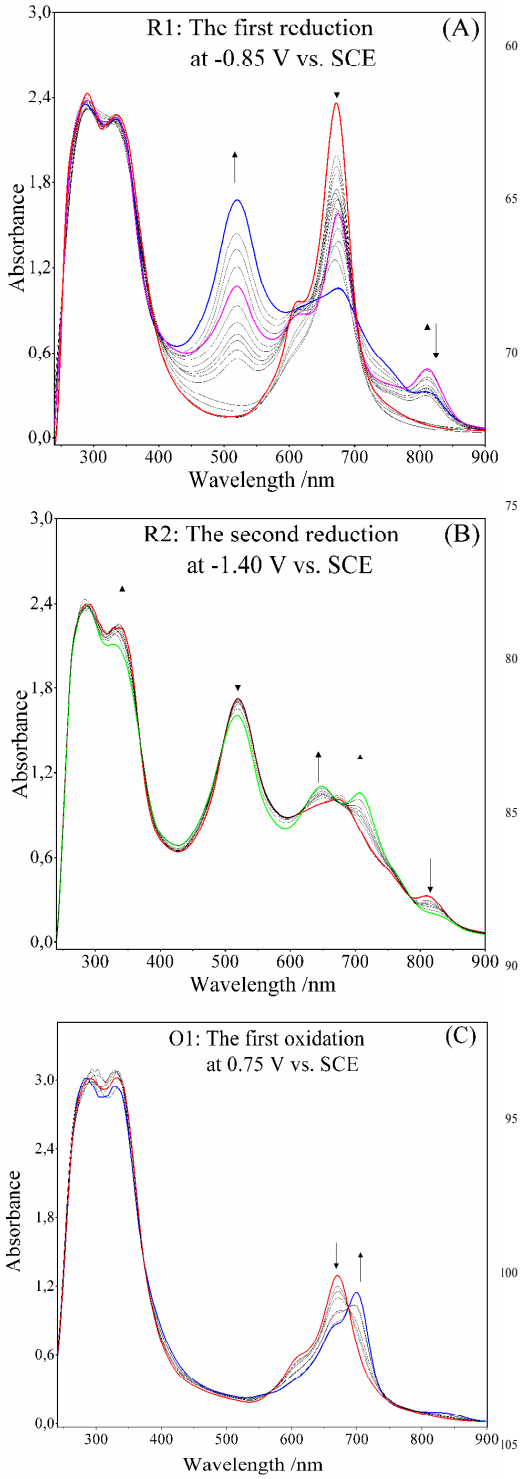

Fig. 2 In situ UV–vis spectral changes during the controlled potential electrolysis of **5** at (A) -0.85 V, (B) -1.40 V and (C) +0.80 V *vs.* SCE.

thus, aggregation–disaggregation equilibrium in solution. On the contrary of the Q-band in the first spectrum of alpha-substituted **5** in Fig. 2A, that in the first spectrum of beta-substituted **6** in Fig. 4A is somewhat broad and blue shifted, which really confirms the presence of the aggregated species of the latter. Therefore, the

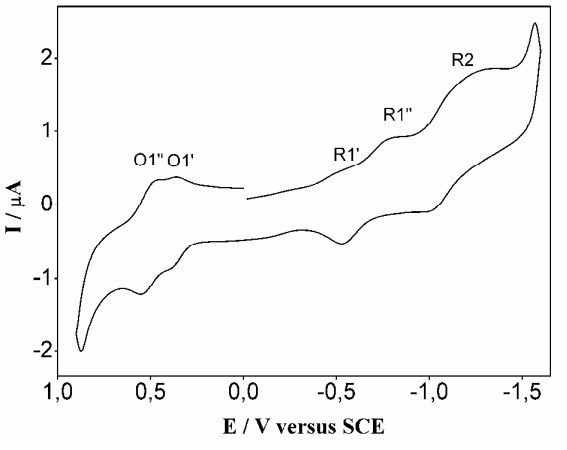

Fig. 3 Cyclic voltammograms of **6** (5.00 x 10^{-4} mole. dm^{-3}) at 0.010 Vs^{-1} on Pt in DMSO/TBAP.

shifting of the band at 632 nm to 656 nm during the first group of *in situ* UV−vis spectral changes monitored through the electrolysis of **6** in deaerated DMSO/TBAP solution at −0.65 V *vs.* SCE, corresponding to the redox process labelled as R1' in Fig. 3 are probably due to chemical exchange associated with the aggregation–disaggregation equilibrium before the first reduction process (Fig. 4A). Further electrolysis of **6** at −0.95 V *vs.* SCE leads to decrease in the Q-band with small red shift and the formation of a new band at 521 nm. These spectral changes are characteristic for the formation of $[Fe(I)Pc(-2)]^-$ species, confirming the CV assignment of the couple R1" to Fe(II)Pc(−2)/

Table 1. The electrochemical data for **5-8**.

Pcs	Redox Processes		[a]$E_{1/2}$ (V vs. SCE)	[b]ΔEp(V)
5	Fe(II)Pc(-2) / [Fe(III)Pc(-2)]	O1	0.51	0.12
	Fe(II)Pc(-2) / $[Fe(I)Pc(-2)]^-$	R1	-0.63	0.11
	$[Fe(I)Pc(-2)]^-$ / $[Fe(I)Pc(-3)]^{2-}$	R2	-1.05	0.12
6	Fe(II)Pc(-2) / [Fe(III)Pc(-2)]	O1′ O1″	(0.37) 0.51	rev
	Fe(II)Pc(-2) / $[Fe(I)Pc(-2)]^-$	[c]R1′ R1″	(-0.53)-0.67	-
	$[Fe(I)Pc(-2)]^-$ / $[Fe(I)Pc(-3)]^{2-}$	R2	-1.13	0.20
7	Fe(II)Pc(-2) / [Fe(III)Pc(-2)]	O1′ O1″	(0.27) 0.60	rev
	Fe(II)Pc(-2) / $[Fe(I)Pc(-2)]^-$	[c]R1′ R1″	(-0.18)-0.40	-
	$[Fe(I)Pc(-2)]^-$ / $[Fe(I)Pc(-3)]^{2-}$	R2′ R2″	(-0.68)-0.90	0.20
8	Fe(II)Pc(-2) / [Fe(III)Pc(-2)]	O1′ O1″	(0.45) 0.60	rev
	Fe(II)Pc(-2) / $[Fe(I)Pc(-2)]^-$	[c]R1′ R1″	(-0.28)-0.50	-
	$[Fe(I)Pc(-2)]^-$ / $[Fe(I)Pc(-3)]^{2-}$	R2	-0.96	0.15

[a]: $E_{1/2}=(E_{pa}+E_{pc})/2$ at 0.010 Vs^{-1}.
[b]: $\Delta E_p= E_{pa}-E_{pc}$ at 0.010 Vs^{-1}.
[c]: $E_{1/2}$ and ΔE_P could not be determined due to ill defined cyclic voltammetry waves, associated with aggregation-deaggregation equilibria.

$[Fe(I)Pc(-2)]^-$ process (Fig. 4B). It is well known from the electrochemical behaviour of Fe(II) Pcs that the reduction

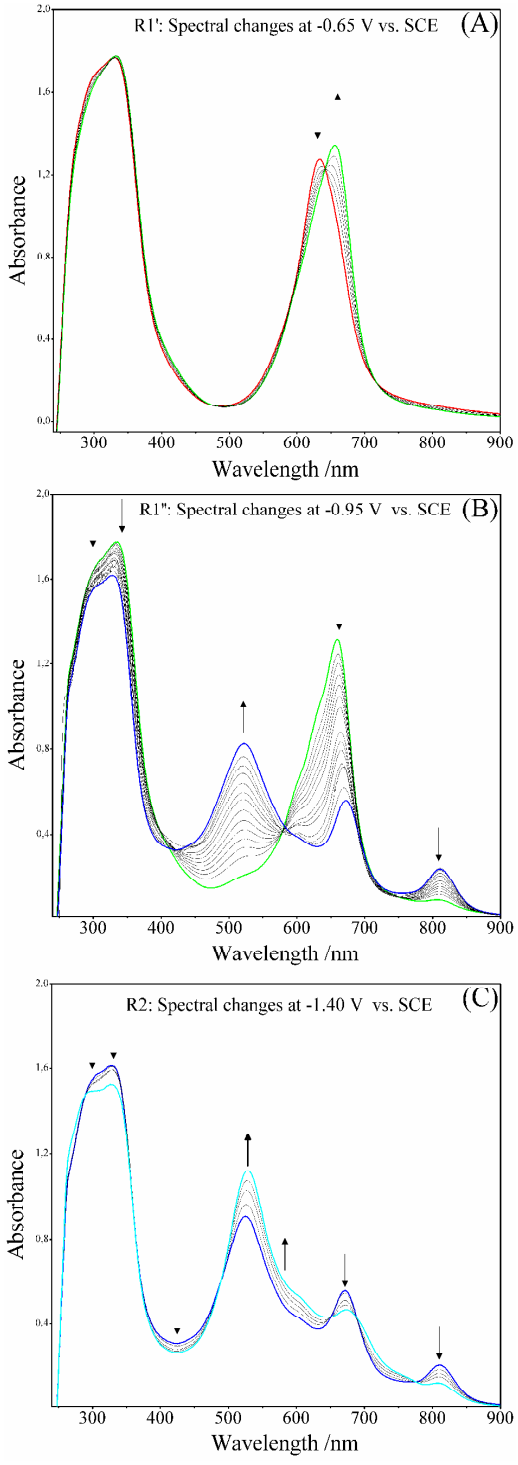

Fig. 4 In situ UV–vis spectral changes during the controlled potential electrolysis of 6 (A) -0.65 V, (B) at -0.95 V and (C) -1.40 V vs. SCE.

processes following the Fe(II)/Fe(I)-based process are ring-based. Thus, the R2 process corresponds to $[Fe(I)Pc(-2)]^-$/ $[Fe(I)Pc(-3)]^{2-}$ couple. The spectral changes in Fig.4C corresponds to this ring-based reduction process. On the other hand, it is clear from the studies in the literature on Fe(II) Pcs that the O1' and O1" couples are metal-based, and correspond to the

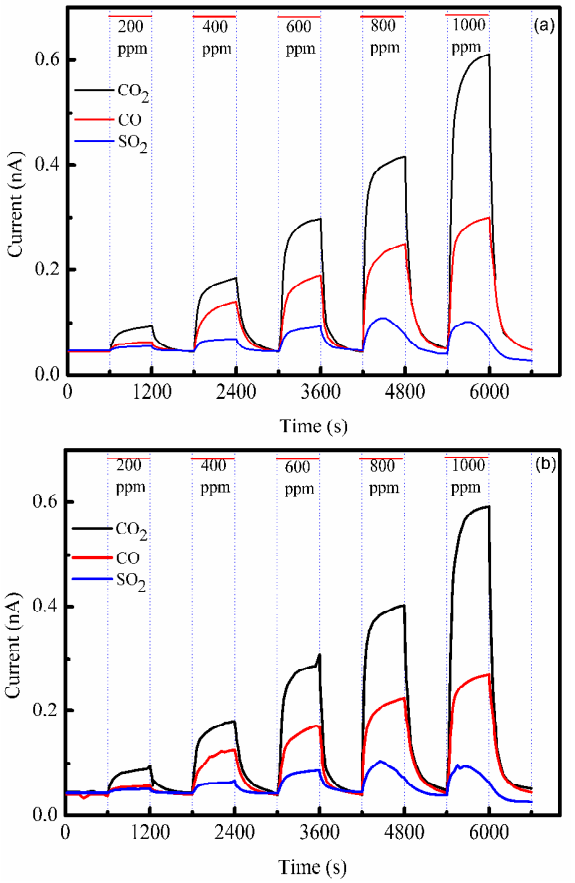

Fig. 5 Comparison of CO_2, CO and SO_2 sensing properties of the **6** coated sensor at 298 K in (a) N_2 and (b) air.

Fe(II)Pc(−2)/[Fe(III)Pc(−2)]$^+$ process of aggregated and nonaggregated species of **6**.[37] The comparison of their electrochemical behaviour shows that the aggregation tendency of the tetra alpha substituted Fe(II)Pc **5** is higher than that of the tetra beta substituted one **6**. This type of behaviour was observed previously in the literature[34,36] and can be attributed to higher planarity of the molecule of **6** than that of **5**. The general redox character of Fe(II)Pc core was not affected significantly by octa substitution instead of beta substitution (Table 1). However, the redox processes of octa substituted Fe(II)Pc complexes (**7** and **8**) shift slightly toward more positive potentials with respect to those of tetra substituted complexes. This shifting can be attributed to easier reduction and more difficult oxidation with increasing number of electron withdrawing coumarin and/or chlorine substituents. The position and the number of substituents, and their electron withdrawing or repelling character were reported in the literature to affect in various ways the redox and aggregation behaviour of metal Pcs compounds.[37-40]

3.3 Gas sensing properties

The sensing properties of the spin coated films of the differently substituted iron(II) complexes **5-8** towards CO_2, CO and SO_2 were carefully examined on the basis of the critical sensing parameters which included dynamic response, sensitivity, and response and recovery time. Figure 5 compares the response-recovery characteristics of the sensor coated with 60 nm film of **6**

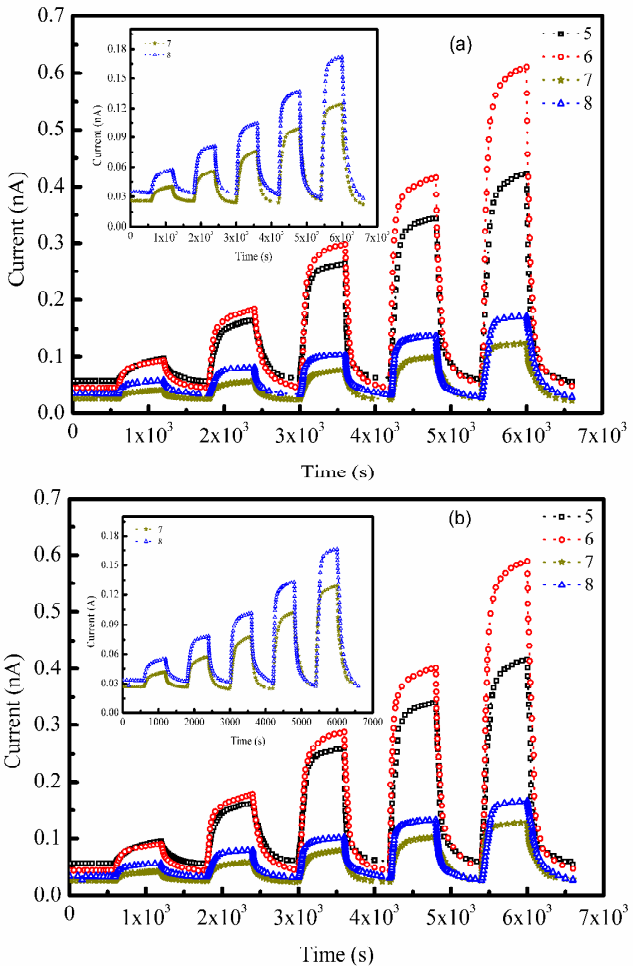

Fig. 6 Response characteristics to 200 – 1000 ppm CO_2 gas of **5-8** based sensors with thickness of 60 nm in (a) N_2 and (b) air at 298 K. (Inset of Fig.6 (a) and (b) show the response characteristics of 7 and 8 coated sensors at an extended scale.)

for various concentrations of CO_2, CO and SO_2 gases at 298 K in (a) N_2 and (b) air. It is clear from this comparison that SO_2 adsorption ability of the compound in both N_2 and air atmosphere is negligibly low, even at a concentration of 1000 ppm. In addition, the sensor current goes through a maximum and then decreases even in the presence of SO_2 gas. The reason for the drop in sensor current in the presence of SO_2 gas is not clear. It is probably associated with a surface process. On the other hand, the exposure of the sensor to various concentrations of CO_2 and CO gases causes a fast increase of sensor current in the initial stage of adsorption. This increase is followed by a drift to the steady state value. After several minutes of exposure to these gases, purging with carrier gas leads to a fast decrease at first, and then, it is followed by a slow drift, and the current reaches finally its initial value after the target gas is turned off. This behavior proves that the adsorption processes are reversible. The same type of response-recovery characteristics were also obtained with other compounds. Furthermore, the results revealed that the SO_2 sensitivity of the compounds is ignorable, which motivated us to study the applicability of the complexes for CO_2 and CO detection. Therefore, the effect of the film thickness and operating temperature on the CO_2 and CO sensing properties of

the films were investigated. The effect of the relative humidity on the CO_2 and CO sensing capability of the spin coated films of the compounds has also been studied. It was found from the thickness dependent measurements that not only the base line current (before exposure to CO or CO_2) but also the sensor sensitivity shows a strong dependence on Pc layer thickness. It was observed that the CO and CO_2 sensitivities decrease while the base line current increases with increasing Pc layer thickness. For example, the initial current values of the films of **8** with 60 and 600 nm thicknesses were about $3.42x10^{-11}$ A and $5.38x10^{-10}$ A, respectively. For all compounds, the sensitivity was observed to increase with the decrease in the film thickness. Therefore, 60 nm thickness was chosen as the optimum film thickness through the experiments. It is well established that the structural arrangement and the overlap of the π-electron systems between the neighbour molecules in the thin film play a fundamental role in the electrical properties of Pc compounds. Therefore, a more reasonable explanation for the increase of the base line current is the change in the degree of crystallinity, grain size and stacking arrangement of the Pc molecules with increasing film thickness. Senthilarasu et al.[41] observed that the degree of crystallinity and grain size increase with the film thickness. The increase in the degree of crystallinity and grain size may result in altering the interaction of the π-electron systems between the different molecules, which may affect the conduction processes in the Pc films. It should be mentioned here that the base line current were dependent on the number of the substituent groups and their positions. The order of initial current values observed for these compounds are **5** > **6** > **8** > **7** at all temperatures investigated.

3.3.1 CO_2 sensing properties of the compounds

The variation of the sensor currents as a function of sensing time for the 60 nm **5-8** coated films at room temperature and exposed to various concentrations of CO_2 gas in N_2 and air is shown in Fig. 6 (a) and (b), respectively. It appears that the interaction of the CO_2 molecules with the spin coated films of **5-8** leads to an increase in sensor current in both N_2 and air (Fig. 6). The rate of increase in the sensor current is high initially; however, it decreases gradually during the later stages of CO_2 detection. The original sensor current is restored approximately 10 minutes after the gas flow is turned off. This behaviour proves that the adsorption processes are reversible. This observation is consistent with the results of Dariani et al.[42] who find that exposure to CO_2 causes a sharp increase in current of 38 nm bromoaluminum Pc thin film, as in our case. Although, the origin of the gas response of a Pc films is not fully understood yet, this effect can be attributed to generating acceptor levels by the CO_2 adsorption. The adsorption of a CO_2 molecule on the Pc layer leads to the creation of an acceptor level near the band edge of the Pc. These acceptor states, which lie below the Fermi level at the initial stage of adsorption, make easy the trapping of valance electrons. When the number of the trapped electrons reaches to a sufficient value, Fermi Level shifts toward to valance band.[43,44] This shift in the Fermi level causes the reduction in the speed of trapping processes, and the rate of increase in current slows down. The exposure of the sensor to carrier gas (dry nitrogen or air) leads to desorption of adsorbed CO_2 molecules from the surface of the active sensing layer, decreasing in the acceptor concentration and thus in the sensor current. The decrease in the rate of increase in the sensor current with time may be attributed to the increase in surface coverage.[45]

The shape of the response and reversal curves in Fig. 6 clearly show that the electrical response of the films exposed to the same concentrations of CO_2 gas is also different depending on the number of the substituent groups and their positions. Although much work has been devoted to the understanding of the adsorption of gas molecules on a solid surface, the adsorption mechanism associated with substituents is still not clear. The relevant factors in the gas/MPc interaction mechanisms are the conjugated π-electron system, the presence of heteroatoms and the central metal atom.[46] In the case of substituted Pcs, the substituents in macrocycle may offer another possible site for complexation. The conjugated π-electron system constitutes a highly polarizable electronic cloud, producing intense dispersion forces between adjacent molecules of Pc. Due to the weak bound of the π-electrons to the Pc molecules, the Pcs are relatively good electron donors. Since the ionization energy of Pcs is low, the energy required for the formation of charge transferred states is also low. The relatively low ionisation energy favours the charge-transfer interactions when electron acceptor molecules are adsorbed onto the Pc surface. It is also believed that the central metal ion together with the peripheral substituents acts as two different sites of interaction with the analyte molecules. Spadavecchia et al. reported in one of their studies that a primary interaction involves the Pc metal and the heteroatom on the analyte molecule while a secondary interaction is determined by the peripheral substituents.[47] On the other hand, the properties of the MPcs, particularly their sensing properties, can be affected by the metal ion coordination and the peripheral attachment of additional atoms or groups that enhance or diminish the ionisation energy.[48] Ma et al. reported that the conductivity of $ZnF_{16}Pc$ increased in the presence of ammonia whereas ZnPc exhibited no or weak sensitivity to this gas.[49] Lee et al. showed that the recovery rate of a tetra-(tert-butyl) substituted CuPc film is superior to that of the unsubstituted CuPc film.[50] It is well known that the electrical conduction processes in Pc compounds depend on several factors that include the chemical nature of Pc, the polymorphic phase of the microcrystallites comprising the film, the film thickness, the presence of impurities or molecular doping and the electrode materials. It is also well known that substituents can change the energetic position of the HOMO or LUMO level, respectively, via mesomeric or inductive effects and the charge carrier injection depends on the energy barrier at the semiconductor metal interface, and is strongly influenced by the structural and electronic properties of the organic films at the contacts.[51] For a particular gas, the intensity and kinetics of the interactions between the Pc films and gas molecules are related to the nature of the Pc compound used as the sensitive material, the charge transport process, relative orientation and separation of adjacent molecules etc. The results obtained here prove that the main role is played by the number of the substituent groups and their positions in the CO_2 gas sensing by 7-oxy-4-(4-methoxyphenyl)-8-methylcoumarin substituted iron(II) Pcs. This finding is consistent with the literature presented above.

The effect of the substituent on the main sensor parameters such as sensitivity (S) for the **5–8** coated sensors was also investigated as a function of CO_2 concentration, film thickness

and temperature. The ratio of the measured current after and before exposing the sensor surface to target gas gives sensitivity,

$$S = \frac{1}{C_i}\frac{\Delta I}{I_0} \quad (1)$$

where ΔI is the changes in current at a concentration of the target gas (C_i) and I_0 is the reference value of the coated devices exposed to carrier gas (dry nitrogen and air in our case). Figure S3 shows the room temperature sensitivity of the 60 nm films of **5-8** coated sensors as a function of CO_2 concentration in (a) N_2 and (b) air. The comparison of the sensor sensitivities in these figures suggests that the type of the carrier gas has practically very small influence on the CO_2 sensitivity of the compounds. As shown in Fig. S3, the sensitivity of the thin films of **5-8** increased approximately linearly with the CO_2 gas within the concentration range of 200–1000 ppm. The sensor designed with beta tetra coumarin substituted complex **6** exhibited significantly higher CO_2 sensitivity than the sensors constructed from **5**, **7** and **8** when tested under identical experimental conditions. For CO_2 at level of 200, 400, 600, 800 and 1000 ppm, the sensitivity of the 60 nm **6** coated sensor is about 5.82×10^{-3}, 7.76×10^{-3}, 9.38×10^{-3}, 1.10×10^{-2} and 1.21×10^{-2} ppm^{-1}, respectively. The slope of the sensitivity–concentration relationship was found to be 7.82×10^{-6} ppm^{-1} in N_2 and 4.80×10^{-6} ppm^{-1} in air for the same compound at room temperature. On the other hand, minimum sensitivity was obtained with **7** involving beta octa coumarin substituent. The room temperature sensitivities of the **6** and **7** coated sensors for CO_2 gas were in the range of $5.82\times10^{-3} - 1.21\times10^{-2}$ and $2.55\times10^{-3} - 3.88\times10^{-3}$ $(ppm)^{-1}$, respectively. It is important to note that the thin film of **6** showed a significant three fold enhancement in sensitivity for all concentrations of CO_2 gas when compared with the results obtained previously by using ball-type dicopper phthalocyanine thin film [42]. At the room temperature, a linear relationship between the sensitivity and CO_2 concentration for **6** coated sensor indicates that the sensors match with linear amplifying circuits for practical application in the detection range of 200-1000 ppm CO_2 gas. The correlation coefficient R^2 of the sensor fit curve was 0.984. In addition, the **5-8** thin film gas sensors were very stable in the high concentration CO_2 gas atmosphere. These results demonstrate that the substituent has influence on the gas sensitivity to some extent.

As a representative result, the variation of the CO_2 sensitivity with film thicknesses for **6** coated sensor in both N_2 and air is shown in Fig. 7 (a) and (b), respectively. It is clear that the CO_2 sensitivity of the film decreases first up to a certain value of the film thickness and then, becomes nearly thickness independent for both carrier gases. The dependence of the sensor sensitivity on the film thickness indicates that the interaction between the sensor and target gases does not involve bulk phenomena. This observation can be attributed to the decrease of the active surface area of the film with increasing film thickness. As the film thickness increases the grain size also increases steadily and reaches a constant value. Thus, a large grain structure gives a smaller adsorption area. The present results also indicate that during the film deposition of each layer, interface states or pores do not form at the interface. This is the reason why the initial current values for thicker films are larger than those for thinner films.

The temperature dependence of the sensitivity for 600 ppm of

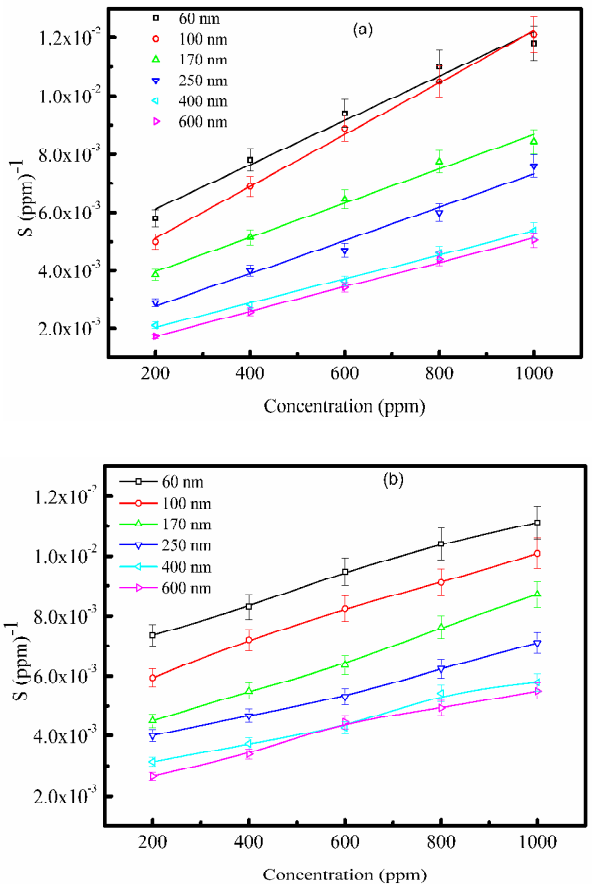

Fig. 7 The dependence of the room temperature (298 K) sensitivity on the film thickness for **6** coated sensor in (a) N_2 and (b) air.

CO_2 gas in (a) N_2 and (b) air is shown in Fig. S4. As shown in this figure, the sensitivity of the films decreases as the testing temperature increases. Similar results on sensitivities have been reported for some other gases coated with different sensing materials.[52] The interpretation of the decrease in sensitivity as the temperature increases requires taking into account many elementary physico-chemical processes. The temperature dependence of the sensitivity suggests that the temperature either decreases the number of active sites on the surface or complicate the adsorption of target molecules into the existing sites. The observed effect can be attributed to the thermally induced structural changes, at least partly.

To compare the response and recovery characteristics of the films, the response and recovery time were estimated from the measured dynamic response characteristics. The response time (τ_{90}) is defined as the time it took the sensor to reach 90% of its saturation value after exposure to a target gas. Likewise, the recovery time (τ_{10}) is defined as the time required returning to 10% below its equilibrium value in carrier gas atmosphere. According to this definition, a small value of response time represents a quick response of the film to CO_2 gas. Figure 8 (a) and 8 (b) show the variation of response and recovery time of the sensors with CO_2 concentration at the room temperature (298 K). On close analysis of the response time plots for these films, it becomes clear that the response time is decreasing function of the

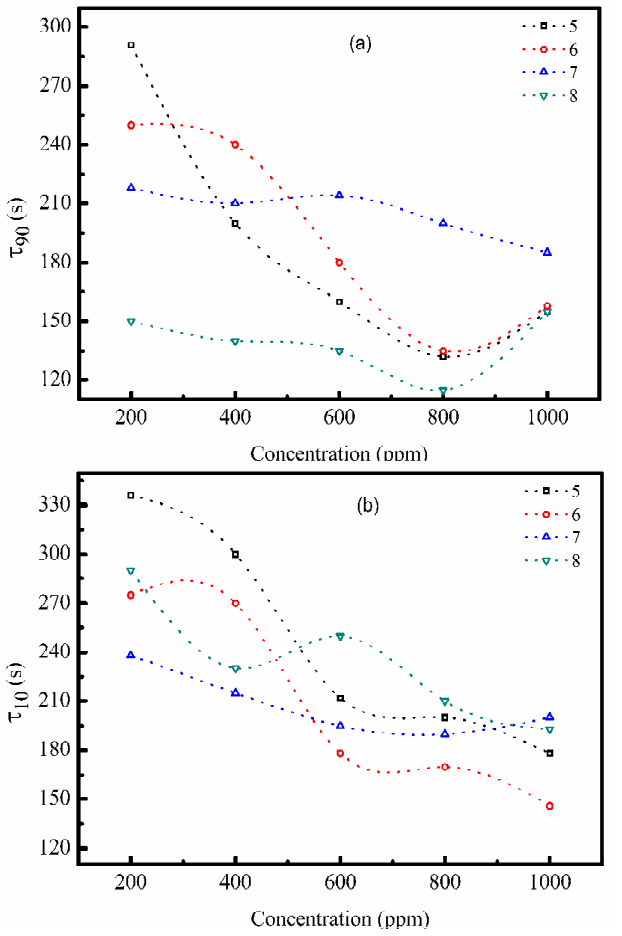

Fig. 8 Variation of response (a) and recovery (b) time of the sensors with CO_2 concentration in N_2 at 298 K.

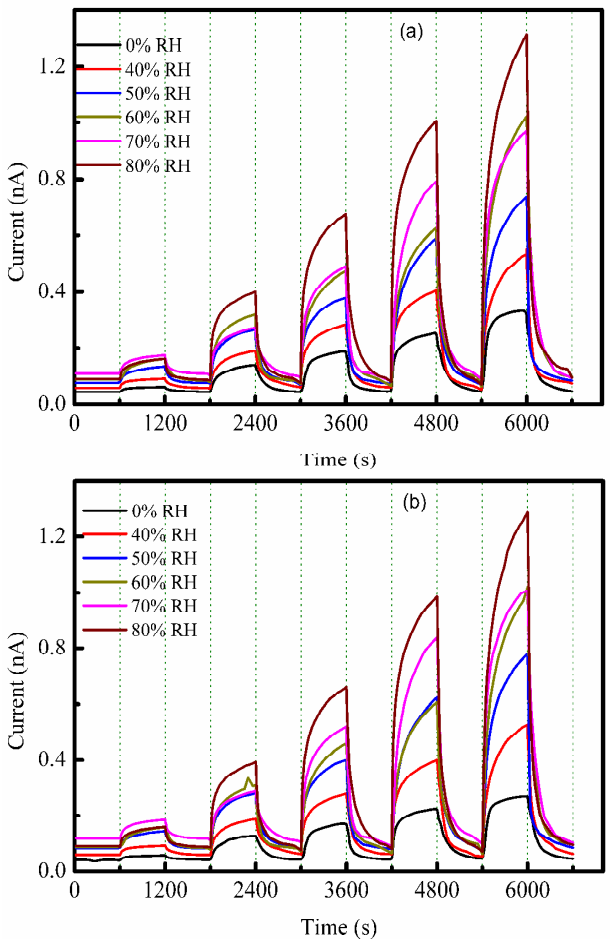

Fig. 9 CO sensing properties of the **6** coated sensor in the condition of different RH at 298 K in (a) N_2 and (b) air.

CO_2 gas concentration for all films. The lowest response time was observed with the **8** coated device for all concentration of CO_2 gas. It was also observed from these measurements that elevation of the sensing temperature leads to a smaller value of response time for all films. Figure 8 (b) shows the variation of the recovery time with CO_2 gas concentrations. It is clear from the figure that the recovery time is also a decreasing function of the gas concentration.

To see the effect of the relative humidity (RH) on the CO_2 sensing properties of the Pc films, the response and recovery characteristics of the sensors were recorded for various RH levels (0%-80%RH). As a representative result, the dependence of the sensing characteristics of the 60 nm **6** coated sensor in the presence of 600 ppm CO_2 on the relative humidity in (a) N_2 and (b) air atmosphere, respectively was shown in Fig. S5. The response and recovery characteristics of the **6** coated sensor in various RH atmosphere appeared to be very similar to that observed in a dry atmosphere (see Fig. 6). The behavior in Fig.S5 shows that the initial value of the sensor current increases with an increase in the RH. It was also observed that CO_2 sensitivity of the sensor decreases with increasing RH for both carrier gases. The humidity dependence of the sensor parameters (S, τ_{90} and τ_{10}) are presented in Table S2. One possible reason to explain the increase in the initial value of sensor current and decrease in sensor sensitivity may be the competitive sorption of CO_2 gas and water molecules on the sensor surface. When the film is exposed to humid atmosphere, before introducing CO_2 gas, the water molecules interact with the film surface, and are adsorbed on it, resulting in an increase of the sensor current. The adsorption of water molecules reduce the number of available sites for CO_2 adsorption and thus, leads to less adsorption of CO_2 molecule on the sensor surface and decrease in sensor sensitivity.

3.3.2 CO sensing properties of the compounds

The effect of relative humidity, functioning as the interference gas, on the response of the sensors used for CO gas detection was evaluated because it is easily expected that the Pc films adsorb not only CO gas but also water vapour. The response characteristics of the sensors in the condition of different RH was also measured with the aim of examining the effect of the relative humidity (RH) on the sensing characteristics of the Pc films. The sensors fabricated using compound **6** as the sensitive layer showed high sensitivity to CO gas, which means that the CO sensing properties of these compounds also depend on the position and the number of substituent groups. Figure 9 shows the response-recovery characteristics of 60 nm **6** film towards five different concentrations of CO under various RH conditions at 298 K in (a) N_2 and (b) air. The plot demonstrates that the film of

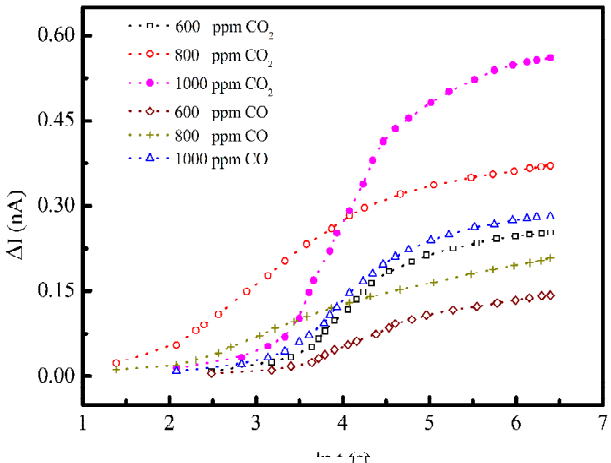

Fig. 10 Plot of ΔI vs. ln (t) according to Elovich equation for compound **6** in dry N_2 atmosphere at 298 K.

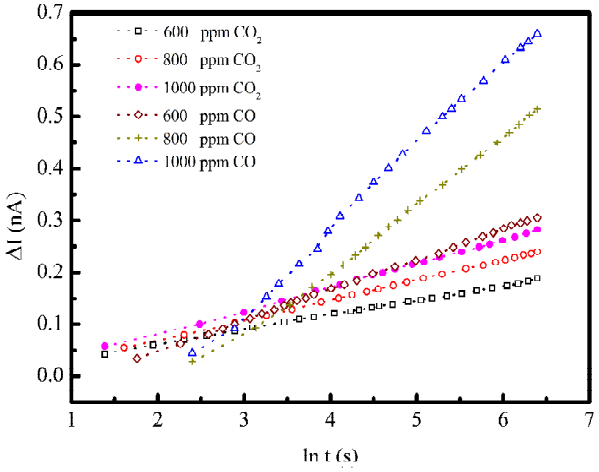

Fig. 11 Plot of ΔI vs. ln (t) according to Elovich equation for compound **6** in humid (50%RH) atmosphere at 298 K.

6 is very sensitive and show very fast response and recovery to the concentrations between 200 and 1000 ppm of CO gas. The baseline current of the **6** film gradually increases from 0.045 nA to 0.110 nA when the RH increases from 0% to 70%. It can be seen from Fig. 9 that CO gas induces similar increase in sensor current as in the case of CO_2. It is quite evident that when switching on CO, the sensor reached saturated current in about 10 min and when switching off, it returned to the original value in about 7 to 8 min. This behaviour proves that the CO adsorption process on the film of **6** is reversible. A possible explanation for the observed CO response of the compounds can be given by the reversible doping process as described for the CO_2 sensing mechanism.

The sensitivity of the sensors to various concentrations of CO gas was determined from the measured response-recovery characteristics using Eq.(1). The average values of main sensor parameters such as sensitivity (S) and response (τ_{90}) and recovery times (τ_{10}) are calculated from the analysis of the measured response-recovery characteristics. As listed in Table S3, the CO sensitivity of the sensor increases with increasing RH. This observation can be related to the catalytically conversion of CO to CO_2. It is also clear from Table S2 that the response time of the sensor is always shorter than recovery time for all RH levels.

3.4 Adsorption kinetics

Adsorption kinetic, which describes the adsorbate adsorption rate, is an important characteristic in evaluating the efficiency of adsorption. A number of equations have been used to describe the kinetics of the adsorption of gas molecules on solids. The kinetics of CO_2 and CO adsorption onto **5-8** was analyzed using Elovich model.

3.4.1. Elovich Model

Elovich equation, in which the interaction between adsorbates is taken into account, has been widely used to describe the adsorption of gas onto heterogeneous solid and adopted to examine the mechanism of the adsorption process. It is also used successfully to describe second order kinetics assuming that the actual solid surfaces are energetically heterogeneous. In reactions involving adsorption of gases on a solid surface, the rate Eq. (3) is commonly used in the kinetics of chemisorption of gases on solids.decreases with time due to an increase in surface coverage. The Elovich equation is generally expressed as[53]

$$\frac{d\theta}{dt} = \alpha \exp(-\beta\theta) \qquad (2)$$

where θ is the sorption capacity at time t, α is the initial sorption rate and β is the desorption constant during any one experiment. To simplify Elovich's equation, Chien and Clayton[54] assumed that $\alpha\beta t >> 1$ and by applying the boundary conditions θ = θ at t = t and θ = 0 at t = 0, the integrated form of Eq. (2) becomes[55]

$$\theta = \left(\frac{1}{\beta}\right)\ln(\alpha\beta) + \left(\frac{1}{\beta}\right)\ln(t) \qquad (3)$$

By assuming that the change in the current (ΔI) is proportional to the change in surface coverage[56], the applicability of Eq. (3) can now be checked by the plot of ΔI vs. ln(t). According to Eq. (3) the plot of ΔI versus ln (t) should result in a straight line. A set of ΔI-ln(t) plots for the adsorption of CO_2 and CO on the compound **6** for some of the experiments at different concentrations of CO_2 and CO in dry atmosphere are shown in Fig. 10. It is clear that the plots have linear regions, but straight lines deviate from linearity and change slope at one, two or three points. It is interesting to note that the number of breaks in the ΔI-ln(t) plots do not depend on the gas concentration. As shown in Fig. 10, the graph splits into three different linear regions for all concentrations of target gases. Similar discontinuities were observed by Taylor et al.[57] in the θ-log t plots for the adsorption of hydrogen on zinc oxide.

It was suggested that if the β is the characteristic of the nature of sites involved in the adsorption, and then the break in the linear plot indicates a change from one kind of site to another. In order to investigate the influence of relative humidity on adsorption kinetics, Elovich model was also employed to CO_2 and CO adsorption on the compounds at various relative humidity. Figure 11 shows the Elovich plot for CO_2 and CO (600 ppm, 800 ppm and 1000 ppm) adsorption on compound **6** in 50% RH atmosphere. It also reveals that, the plots of ΔI versus ln (t)

are linear for all concentrations of CO_2 and CO gases investigated, indicating that the interaction obeys the Elovich equation.

Conclusions

The iron(II) Pcs **5**, **6**, **7** and **8** have been synthesized by the reaction of iron(II)acetate salt with 3-(4-(4-methoxyphenyl)-8-methyl-coumarin-7-oxy)phthalonitrile **1**, 4-(4-(4-methoxyphenyl) -8-methylcoumarin-7-oxy)phthalonitrile **2**, 4-chloro-5-(4-(4-methoxyphenyl)-8-methylcoumarin-7-yloxy)phthalonitrile **3** and 4,5-bis(4-(4-methoxyphenyl)-8-methylcoumarin-7-loxy)phthalonitrile **4**, respectively. The compounds were characterized by UV–vis, IR and MALDI-TOF mass spectrometry, and elemental analysis. The electronic absorption spectra of the iron(II)Pc compounds showed that aggregation tendencies of **6** and **7** are higher than those of **5** and **8**. The electrochemical and *in situ* spectro-electrochemical measurements of tetra beta, tetra alpha and octa beta coumarin substituted iron(II)Pcs showed that these compounds display both metal- and Pc ring-based redox proceses. Furthermore, it was concluded that aggregation and redox behaviour of these complexes are affected by the position and the number of substituents, and their electron withdrawing or repelling character. The effect of concentration, operating temperature and humidity, acting as interference gas, on the gas sensing properties of these compounds were studied and discussed. The thin films of the compounds **5**-**8** in fabricated gas sensors showed high sensitivity to CO_2 depending on the substituent group even at room temperature. The results of the sensing measurements illustrated the importance of the number and type of substituents in the Pc ring in term of the modulation of the sensors' response. The sensitivity and the response time of the sensors were strongly dependent on temperature. The substituent dependence in gas sensing performance and electrical behaviour of the devices suggested that band structures of the Pc films were modified significantly by the change in the number and position of the substituents. The nature of interaction of the investigated films with CO_2 and CO molecules was discussed in terms of Elovich models. In dry atmosphere, the linear regression values obtained from the Elovich kinetic model were lower than humid environment.

Acknowledgments

We are thankful to Marmara University, The Commission of Scientific Research Projects (BAPKO) (Project No: FEN-C-DRP-101013-0406 and FEN-A-130511-0159) and The Turkish Academy of Sciences (TUBA) for their financial support. This work was also supported by the Yıldız Technical University Commission of Scientific Research Projects under Grant No. 2014-01-01-YL01 and 2014-01-01-KAP01. One of the authors (A. Altındal) is thankful to the Scientific Research Commission of Yıldız Technical University.

Notes and references

[a] *Department of Chemistry, Marmara University, 34722 Göztepe, Kadıköy, Istanbul, Turkey. Fax:+90 216 3478783; Tel: +90 216 3479641; E-mail: selcukaltun@marmara.edu.tr, efeorman@marmara.edu.tr, zodabas@marmara.edu.tr, aliozkaya@marmara.edu.tr.*

[b] *Department of Physics, Yıldız Technical University, 34210 Esenler, Istanbul, Turkey. Fax:+90 212 383 42 34; Tel: +90 212 383 42 31; E-mail: altindal@yildiz.edu.tr.*

† Electronic Supplementary Information (ESI) available: [details of any supplementary information available should be included here]. See DOI: 10.1039/b000000x/

1 N.B. Mckeown, *Phthalocyanine Materials:* Cambridge University Press: Cambridge, 1998.
2 C.Y. Ma, K.Q. Ye, S.K. Yu, G.T. Du, Y.F. Zhao, F.D. Cong, Y.C. Chang, W.H. Jiang, C.H. Cheng, Z.Q. Fan, H.F. Yu, W.C. Li, *Dyes Pigm.*, 2007, **74**, 141.
3 Y. Arslanoglu, E. Hayran, E. Hamuryudan, *Dyes Pigm.,* 2013, **97**, 340.
4 Z. Odabaş, E.B. Orman, M. Durmuş, F. Dumludağ, A.R. Özkaya, M. Bulut, *Dyes Pigm.,* 2012, **95**, 540.
5 C.C. Leznoff, A.B.P. Lever (Eds.), *Phthalocyanines: Properties and Applications,* vol. 1–4, VCH Publishers, New York, 1989, 1993, 1996.
6 N.B. McKeown, *Phthalocyanine Materials:* Cambridge University Press, Cambridge, 1998.
7 N. Grootboom, T. Nyokong, *J. Mol. Catal. A: Chem.,* 2002, **179**, 113.
8 K. Ozoemena, T. Nyokong, *Electrochim. Acta,* 2002, **47**, 4035.
9 A.A. Kuznetsova, L.I. Solovyeva, O.L. Kaliya, E.A. Lukyanets, D.G. Knorre, O.S. Fedorova, *Bioorg. & Med. Chem. Lett.,* 2009, **19**, 4335.
10 N. Leidel, A. Popovic-Bijelic, K.G.V. Havelius, P. Chernev, N. Voevodskaya, A. Graslund, M. Haumann, *Biochim. et Biophys. Acta,* 2012, **1817**, 430.
11 O.O. Fashedemi, K.I. Ozoemen, *Sens. Actuators B,* 2011, **160**, 7.
12 R. Baker, D.P. Wilkinson, J. Zhang, *Electrochim. Acta,* 2008, 53, 6906.
13 F.A. Walker, U. Simonis, in: L.J. Berliner, J. Reuben (Eds.), *Encyclopedia of Inorganic Chemistry,* Plenum Press, New York, 1993, pp. 133–274.
14 G. Guillaud, J. Simon, J.P. Germain, *Coord. Chem. Rev.,* 1998, **180**, 1433.
15 K. Kadish, K.M. Smith, R. Guilard, *The Porphyrin Handbook,* Academic Press, Boston, 1998.
16 H. Ali, J.E. Van Lier, *Chem. Rev.,* 1999, **99**, 2379.
17 K. Morishige, S. Tomoyasu, G. Iwani, *Langmuir*, 1997, **13**, 51184.
18 F.H. Moser, L.R. Thomas, *Phthalocyanine Compounds,* Reinhold, New York,1963, pp. 123–145.
19 T. Tominaga, K. Hayashi, N. Toshima, *J. Porphyr. Phthalocya.,* 1997, **1**, 239.
20 M.A.T. Gilmartin, J.P. Hart, D.T. Patton, *Analyst,* 1995, **120**, 1973.
21 M.J. Cook, I. Chambrier, S.J. Cracknell, D.A. Mayes, D.A. Russel, *Photochem. Photobiol.,* 1995, **62**, 542.
22 A. Kotali, I.S. Lafazanis, P.A. Haris, *Tetrahed. Lett.,* 2007, **48**, 7181.
23 Duarte, F. J. and L. W. Hillman (Eds.). Dye Laser Principles, Academic: New York, 1990.
24 F.F. Ye, J.R. Gao, W.J. Sheng, J.H. Jia, *Dyes Pigm.,* 2008, **77**, 556.
25 M. Pişkin, M. Durmuş, M. Bulut, *Spectrochim. Acta Part A: Mol. Biomol. Spect.,* 2012, **97**, 502.
26 A.A. Esenpınar, E. Durmaz, F. Karaca, M. Bulut, *Polyhedron*, 2012, **38**, 267.
27 E. Dur, M. Bulut, *Polyhedron*, 2010, **29**, 2689.
28 Z. Odabaş, H. Kara, A.R. Özkaya, M. Bulut, *Polyhedron,* 2012, **39**, 38.
29 S. Altun, A.R. Özkaya, M. Bulut, *Polyhedron,* 2012, **48**, 31.
30 S. Altun, Z. Odabaş, A. Altındal, A.R. Özkaya, *Polyhedron Dalton Trans.*, 2014, 43.
31 M. Çamur, A.R. Özkaya, M. Bulut, *Polyhedron*, 2007, **26**, 2638.
32 M. Özer, A. Altındal, A.R. Özkaya, Ö. Bekaroğlu, *Dalton Trans.,* 2009, **17**, 3175.
33 J. Houghton, *Env. Protect. Bull.,* 2002, **66**, 21.
34 A. Alemdar, A.R. Özkaya, M. Bulut, *Synth. Met.,* 2010, **160**, 1556.
35 A. Günsel, M. Kandaz, A. Koca, B. Salih, *Polyhedron,* 2011, **30**, 1446.

36 A. Alemdar, A.R. Özkaya, M. Bulut, *Polyhedron,* 2009, **28**, 3788.
37 M. Arıcı, D. Arıcan, A.L. Uğur, A. Erdoğmuş, A. Koca, *Electrochim. Acta,* 2013, **87**, 554.
38 D. Arıcan, M. Arıcı, A.L. Uğur, A. Erdoğmuş, A. Koca, *Electrochim. Acta,* 2013, **106**, 541.
39 M. Canlıca, I.N. Booysen, T. Nyokong, *Polyhedron,* 2011, **30**, 508.
40 M. Canlıca, I.N. Booysen, T. Nyokong, *Polyhedron,* 2011, **30**, 522.
41 S. Senthilarasu, Y.B. Hahn and S.H. Lee, *J. Appl. Phys.,* 2007, **102**, 043512.
42 M.E. Azim-Araghi, Z. Bisadi, R.S. Dariani, *Proceedings of the 4th International Conference on Nanostructures (ICNS4),* 12-14 March, 2012, Kish Island, I.R. Iran.
43 A. Altındal, Ö. Kurt, A. Şengül, Ö. Bekaroğlu, *Sens. and Actuators B.,* 2014, **202**, 373.
44 L. Grządziel, J. Żak, J. Szuber, *Thin Solid Films*, 2003, **436**, 70.
45 C. Aharoni, F.C. Tompkins, *Advances in Catalysis and Related Subjects,* In: D.D. Eley, H. Pines, P.B. Weisz (Eds.), vol. 21, Academic Press, New York, 1970, pp. 1–49.
46 T. Basova, E. Kol'tsov, A.K. Ray, A.K. Hassan, A.G. Gürek, V. Ahsen, *Sens. Actuators B,* 2006, **113**, 127.
47 J. Spadavecchia, G. Ciccarella, R. Rella, *Sens. Actuators B*, 2005, **106**, 212.
48 A.M. Paoletti, G. Pennesi, G. Rossi, A. Generosi, B. Paci, V.R. Albertini, *Sensors,* 2009, **9**, 5277.
49 M. Xingfa, C. Hongzheng, S. Minmin, W. Gang, W. Mang, H. Ji, *Thin Solid Films,* 2005, **489**, 257.
50 Y.L. Lee, C.Y. Sheu, R.H. Hsiao, *Sens. Actuators B.,* 2004, **99**, 281.
51 G. Horowitz, *J. Mater. Res.,* 2004, **19**, 1946.
52 A. Qureshi, A. Altındal, A. Mergen, *Sens. Actuators B.,* 2009, **138**, 71.
53 M.J.D. Low, *Chemical Reviews,* 1960, **60**, 267.
54 S.H. Chien, W.R Clayton, *Soil Sci. Soc. Am. J.,* 1980, **44**, 265.
55 D.L. Sparks, *Soil Physical Chemistry,* in: D.L. Sparks (Ed.), CRC Press, Boca Raton, Florida, 1986, pp. 83–145.
56 J.W. Gardner, M.Z. Iskandarani, B. Bott, *Sens. Actuators B.,* 1992, **9**, 133.
57 H.A. Taylor, N. Thon, *J. Am. Chem. Soc*., 1952, **74**, 4169.

The synthesis of novel alpha tetra, beta tetra and beta octa 4-(4-methoxyphenyl)-8-methyl-coumarin-7-oxy, and beta octa 4-chloro-5-(4-(4-methoxyphenyl)-8-methylcoumarin-7-oxy substituted iron(II) phthalocyanines has been achieved by the reaction of corresponding phthalonitriles with iron(II)acetate. The compounds were characterized by elemental analysis, FT-IR, UV–*vis*, and MALDI-TOF mass spectrometry. The reduction and oxidation properties of the compounds were identified by voltammetric and *in situ* spectroelectrochemical measurements. The gas sensing behavior of the spin coated films of the differently substituted iron(II) complexes towards CO_2, CO and SO_2 were investigated at various temperatures between 300 K and 500 K. While exposure to SO_2 had no considerable influence on the sensor current, the presence of CO and CO_2 gases led to large increase in sensor currents. The effect of relative humidity on the CO and CO_2 sensing capability of the spin coated films was also studied. The results showed that the presence of water vapor, acting as interference gas, causes a decrease of the CO_2 sensitivity, but an increase of the CO sensitivity of the sensors. The experimental adsorption data were analyzed using Elovich kinetic model. Linear regression analysis results show that Elovich equation provides the best correlation for the CO_2 and CO adsorption processes under humid conditions. However, the experimental data deviated considerably from the theoretical model in dry atmosphere.